Journal of Physics and Chemistry of Solids 182 (2023) 111568

Contents lists available at ScienceDirect

Journal of Physics and Chemistry of Solids

journal homepage: www.elsevier.com/locate/jpcs

# Synthesis, structure and canted antiferromagnetism of layered cobalt hydroxide sorbate

Jonathan B. Lefton [a,1], Wenhao Liu [b], Claire McGuire [a], Bing Lv [b], Craig M. Brown [c,d], Ryan A. Klein [d,e,*,1], Tomče Runčevski [a,**]

[a] Department of Chemistry, Southern Methodist University, Dallas, TX, 75205, USA
[b] Department of Physics, University of Texas at Dallas, Richardson, TX, 75080, USA
[c] Department of Chemical and Biomolecular Engineering, University of Delaware, Newark, DE, 19716, USA
[d] NIST Center for Neutron Research, National Institute for Standards and Technology, Gaithersburg, MD, 20899, USA

ARTICLE INFO

*Keywords:*
Layered hydroxides
Crystal structure
Magnetism
Powder diffraction
Rietveld refinement

ABSTRACT

Layered hybrid organic–inorganic compounds of the transition metal hydroxides, in which part of the hydroxide ions are exchanged for organic ligands that act as spacers of the 2-dimensional inorganic layers, elicit new or enhanced properties. The interlayer ligands enable fine-tuning of the physicochemical properties of the metal hydroxide layers, including their magnetism. Specifically, within the $Co(OH)_2$ family of transition ion hydroxides, this approach has been leveraged to stabilize antiferromagnetic and ferrimagnetic ground states for pillared and layered complexes, respectively. Here, we further investigate the effects of changing dimensionality, local Co coordination, and interlayer spacing on the magnetic ground state of brucite-like $\beta$-Co(OH) layered complexes. We report the hydrothermal synthesis of a new crystalline material, Co(OH)(sorb), where the inorganic layers are spaced by monotopic, doubly unsaturated sorbate ligands (sorb = $[C_6H_7O_2]^-$). The material was structurally characterized using powder X-ray and neutron diffraction measurements and the crystal structure was solved *ab initio* from powder diffraction data and refined using the Rietveld method. The magnetic susceptibility and magnetization measurements reveal canted antiferromagnetic ordering with $T_N = 41.7$ K. This report augments our understanding of tuning magnetism through dimensionality in layered complexes and represents a step forward in the design of new 2D layered hybrid compounds.

## 1. Introduction

Metal hydroxides are ubiquitous in society today, with applications ranging from energy storage and renewable energy generation to catalysis [1–5]. Incorporating organic ligands into the parent metal hydroxide structures allows for synthetic tuning of dimensionality in these materials and can lead to compounds with well-defined 2D inorganic layers. Such hybrid layered organic-inorganic materials often have new or enhanced physicochemical properties compared to the pure metal hydroxide parent materials [6,7]. Indeed, hybrid layered metal hydroxides are shown to be promising new materials in catalysis [8], gas sorption [9], photoswitches [10], pseudocapacitors [11],supercapacitors [12], and magnetic cooling [13,14]. The organic ligands are highly modular, which creates a huge synthetic phase space for new materials with tailored properties for specific end use applications.

One particularly interesting transition metal hydroxide is cobalt(II) hydroxide, $Co(OH)_2$, which has two distinct polymorphs. Of these, $\beta$-$Co(OH)_2$ is stable at ambient conditions, and, like bulk CoO [15,16], it is an antiferromagnet. $\beta$-$Co(OH)_2$ has a layered brucite-type structure (Fig. 1) and the material displays a substantial magnetocaloric effect, making it potentially useful for magnetic cooling applications [17–19]. Several successful methods have been employed to further tune the magnetism in $Co(OH)_2$ by modifying the structure and dimensionality [20–30]. The layered nature of this metal hydroxide positions it as a good target for creating new layered hybrid compounds and for exploring the relationship between magnetism, emergent phenomena, and dimensionality

e Material, Chemical, and Computational Sciences Directorate, National Renewable Energy Laboratory, Golden, CO, 80401, USA
* Corresponding author. NIST Center for Neutron Research, National Institute for Standards and Technology, Gaithersburg, MD, 20899, USA.
** Corresponding author.
*E-mail addresses:* ryan.klein@nrel.gov (R.A. Klein), truncevski@smu.edu (T. Runčevski).
[1] R.A.K. and J.B.L contributed equally to this work. The authors declare no competing financial interest.

https://doi.org/10.1016/j.jpcs.2023.111568
Received 2 March 2023; Received in revised form 11 June 2023; Accepted 18 July 2023
Available online 24 July 2023
0022-3697/Published by Elsevier Ltd.

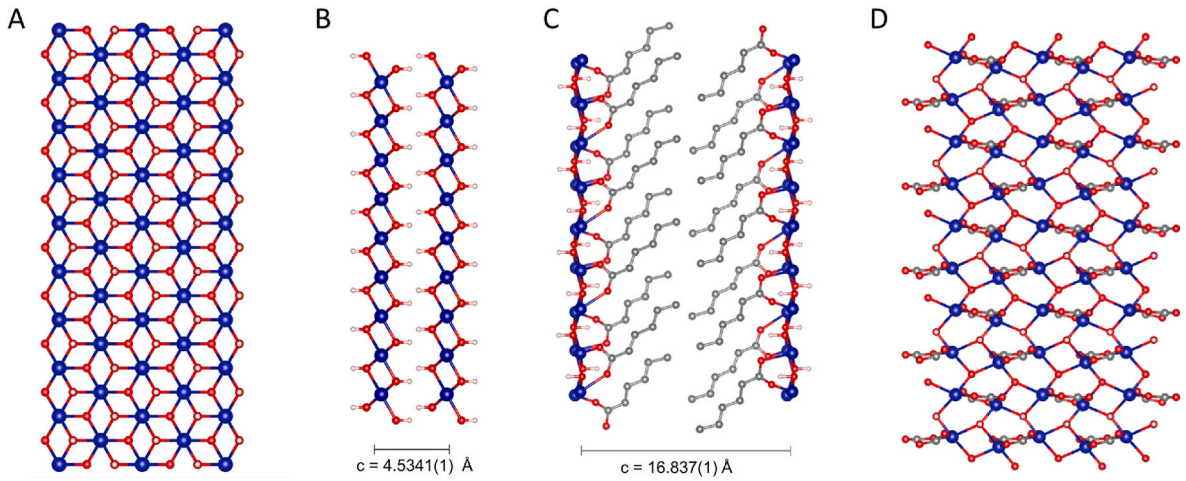


**Fig. 1.** Crystal structures of the Co(OH) layers and interlayer spacing in (A,B) $\beta$-$Co(OH)_2$ and (C,D) Co(OH)(sorb) as determined from powder neutron diffraction measurements at 100 K. Blue, red, white, and gray spheres depict Co, O, H, and C atoms, respectively. Values in parentheses indicate $\pm 1\sigma$.

in this class of materials.

The choice of linker to generate the new hybrid material determines the resulting physicochemical properties, like the magnetism, in these materials compared to bulk $\beta$-$Co(OH)_2$.[19] The linkers can be monotopic and separate the adjacent Co(OH) layers or they can be ditopic/multitopic and bridge adjacent Co(OH) layers. For example, an ethanedisulfonate-pillared cobalt hydroxide, $Co_3(OH)_4(O_3SCH_2CH_2SO_3)$, is shown to be antiferromagnetic ($T_N = 38$ K, $\theta_{CW} = -243$ K), with a field induced ferrimagnetic transition at 0.1 T [31]. Similarly, a ditopic 1,4-benzenedicarboxylate-based cobalt hydroxide material, $Co_2(OH)_2$(bdc), (bdc = 1,4-benzenedicarboxylate, $C_8H_4O_4$, also called terephthalate) exhibits antiferromagnetism ($T_N = 48$ K) with field-induced spin canting between layers that leads to a giant magnetic hysteresis effect at 4.2 K with $H_C = 5.9$ T [29,32]. Alternatively, monotopic ligands separate the Co(OH) layers. The resulting separated layers are held together by relatively weak non-covalent interaction, which affects the magnetism in these systems. For example, a monotopic cinnamate-based ligand was used to produce a hybrid cobalt hydroxide, $Cu(C_9H_7O_2)_{0.8}(OH)_{1.2}$, that possesses ferrimagnetic long-range ordering ($T_C = 47.5$ K, Curie constant $C = 2.51$ emu K $mol^{-1}$) and large hysteresis in the magnetization data with the coercive field $H_C = 3.8$ T at 2 K [28].

As such, hybrid layered cobalt hydroxides exhibit proximity between antiferromagnetic and ferrimagnetic ground states and it appears that the ground state is selected by the choice of organic linker. Further investigation is warranted to better understand the effects of dimensionality, interlayer spacing, and local coordination at the Co ions on the magnetic properties in these transition ion hydroxide hybrid materials.

Here, we select sorbic acid as the organic ligand for the synthesis of a new hybrid metal cobalt hydroxide material. Sorbic acid ($C_6H_8O_2$) is a monotopic, doubly conjugated linker which we hypothesized could generate a hybrid material with weak interactions between the Co(OH) layers [33]. The bidentate nature of the carboxylate moiety might help generate a modified Co(OH) layer structurally reminiscent of β-$Co(OH)_2$. In addition, the doubly unsaturated hydrocarbon backbone offers another handle for further post-synthetic modifications such as halogenation [34], *cis-trans* isomerization, and 2 + 2 dimerization or polymerization by heat, light, or pressure [35]. The terminal methyl groups on the sorbate may also lead to weak interlayer van der Waals interactions. As such, we hypothesized that this material may lend itself to exfoliation to yield isolated single layers of brucite-like Co(OH) sandwiched between hydrophobic organic linkers.

Hydrothermal synthesis of Co(OH)(sorb) (sorb = $[C_6H_7O_2]^-$) yielded bundled needle-shaped microcrystals as visualized by scanning electron microscopy (SEM) measurements. We structurally characterized the compound using powder X-ray diffraction (PXRD) and powder neutron diffraction (PND) measurements. The vibrational spectroscopic properties of Co(OH)(sorb) were studied by Fourier-transform infrared (FTIR) spectroscopy measurements. More interestingly, Zero-field cooled (ZFC) and field cooled (FC) magnetic susceptibility and magnetic hysteresis measurements revealed that Co(OH)(sorb) is a canted antiferromagnet with a large hysteresis of 2.5 T at 10 K. Thermogravimetric analysis (TGA) was used to study the thermal decomposition pathway, revealing stepwise mass-loss to metallic Co(0) at 1273 K. Lastly, the possible application of Co(OH)(sorb) as a precursor for the synthesis of cobalt nanoparticles was probed through post thermal degradation and subsequent PXRD and SEM measurements.36.

## 2. Experimental section

**Materials.** Cobalt(II) nitrate hexahydrate (Acros Organics[2], 99% purity), cobalt(II) hydroxide (Strem, 97% purity), sorbic acid (TCI, >99% purity) and potassium sorbate (Alfa Aesar, 99% purity), were handled in air, and used as received.

**Hydrothermal synthesis.** Cobalt nitrate hexahydrate (7.28 g, 25.0 mmol) and potassium sorbate (7.51 g, 50.0 mmol) were added to a 1 L bottle with 500 mL of deionized water. The solution was sparged with nitrogen gas for 1 h, then sealed with a lid and placed into an 80 °C oven for 24 h. A pink solid formed and was collected by hot filtration, washed several times with deionized water, and then dried overnight in air. The resulting product (1.15 g, 25% yield) was characterized using PXRD, PND, SEM, TGA, SQUID-based magnetometry, and FTIR spectroscopic measurements. Further figures and experimental details, including details of the Pawley fits and Rietveld refinements for the PXRD and PND patterns, the FTIR spectra, and TGA analysis can be found in the Supporting Information.

**PXRD.** Powder X-ray diffraction data were collected at room temperature using a laboratory Stoe Stadi-P powder diffractometer, operating in Debye−Scherrer geometry, equipped with a molybdenum X-ray source and monochromatic Mo-$K\alpha_1$ radiation obtained by a primary Ge (111) monochromator. Two linear position sensitive silicon-strip (Mythen Dectris 1K) detectors were used to record the scattered X-ray intensity. The crystalline powder was packed in a borosilicate capillary with 0.5 mm diameter. The capillary was rotated during the

[2] Certain commercial equipment, instruments, or materials (or suppliers, or software, …) are identified in this paper to foster understanding. Such identification does not imply recommendation or endorsement by the National Institute of Standards and Technology, nor does it imply that the materials or equipment identified are necessarily the best available for the purpose.

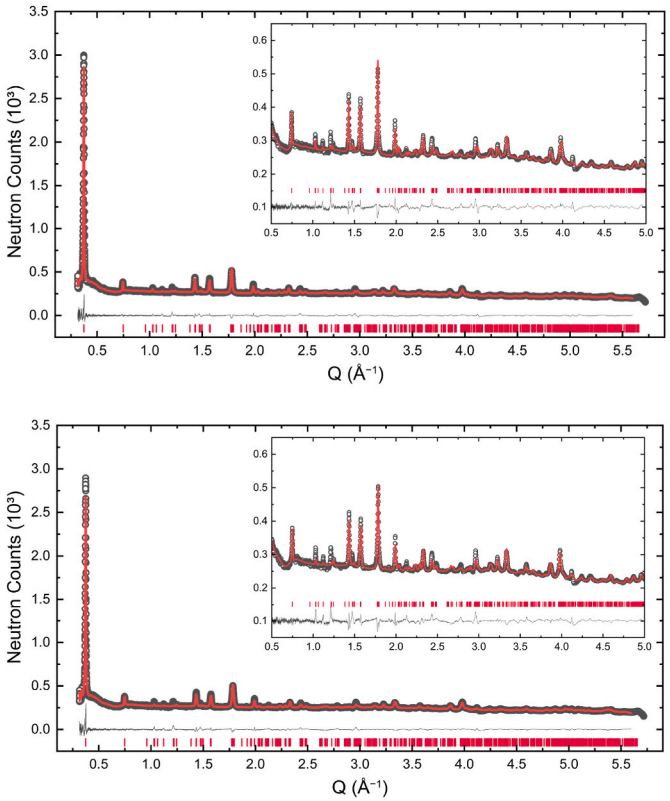


**Fig. 2.** Rietveld refinement fits for the $P2_1$ model without rigid bodies for the linkers of the PND pattern for Co(OH)(sorb) collected at 100 K (top) and 6.71 K (bottom). The insets show the fits to the data between Q = 0.5 Å$^{-1}$ and Q = 5.0 Å$^{-1}$. Black circles, red curves, gray curves, and red tick marks denote the data, Rietveld refinement curves, difference curves, and *hkl* positions, respectively. Symbols are commensurate with error bars which indicate ±1σ. Fit statistics at 100 K and 6.71 K are $R_{exp}$ = 0.450%, $R_{wp}$ = 1.848%, $R_p$ = 2.055%, GOF = 4.110; $R_{exp}$ = 0.441%, $R_{wp}$ = 1.811%, $R_p$ = 2.209%, GOF = 4.111, respectively.

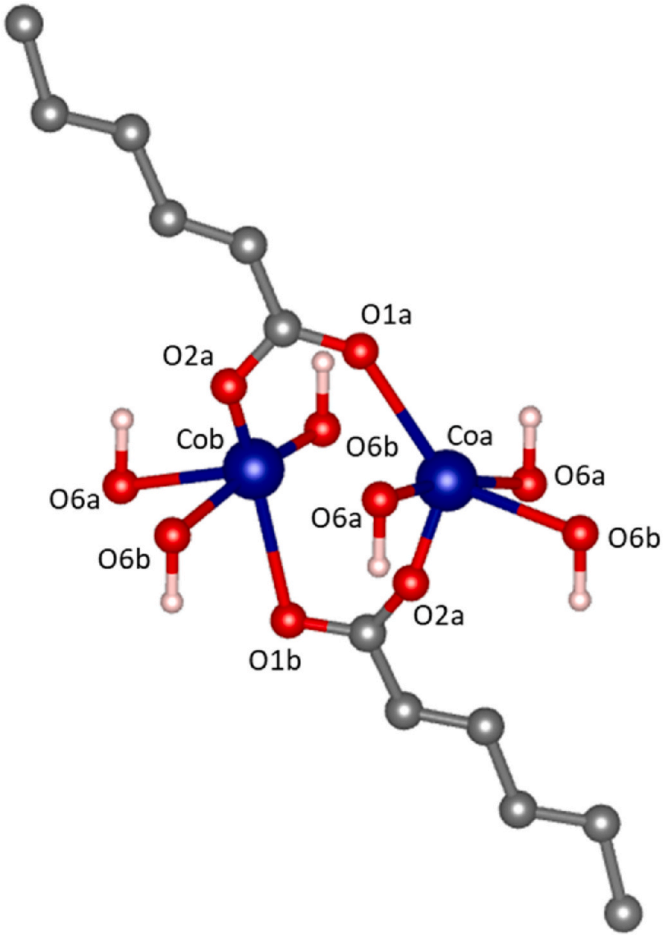


**Fig. 3.** A fragment of the crystal structure of Co(OH)(sorb) is shown here depicting the coordination of the Co centers. The structure derives from a Rietveld refinement of the PND pattern collected at 100 K. Blue, red, gray, and white spheres depict Co, O, C, and H atoms, respectively.

measurement for better particle statistics.

**PND.** In a He-filled glove box, 0.9739 g crystalline powder were loaded into a vanadium sample can (inner diameter = 6 mm) and sealed using a Cu gasket. PND patterns were collected using the high-resolution time-of-flight powder diffractometer (POWGEN) at the Spallation Neutron Source (SNS), Oak Ridge National Laboratory (ORNL). Data were collected for ≈3 h for each pattern using a center wavelength of λ = 2.665 Å at T = 6.71 K and 100 K in a scattering vector range from d = 1.1 Å to d = 20.5 Å (d = 2πQ$^{-1}$).

**SEM.** The microscope images (Fig. 6) were collected on a JEOL Field Emission Scanning Electron Microscope (FE-SEM) IT500HR. Analytical Working Conditions: Vacuum in variable pressure (60–70Pa) 15 kV high voltage, Beam Current ≈ 50 nA, 10 mm working distance.

**FTIR.** Infrared spectra (Fig. S1) were collected on a ThermoScientific Nicolet iS5 Fourier-Transform Infrared Spectrophotometer with a iD7 Attenuated Total Reflectance (ATR) accessory, and was treated with a baseline correction.

**TGA.** The analysis (Fig. S4) was performed on a Netzsch TG 209 F3 Tarsus instrument, measuring from 298 K to 1273 K at a rate of 10 K/min, in an alumina crucible under constant flow of nitrogen gas. An empty crucible was measured as a baseline.

## 3. Results & discussion

**Structure solution and refinement.** The powder diffraction patterns were analyzed using TOPAS Academic [37], CMPR [38], and GSAS/EXPGUI software packages [39,40]. The sample was structurally characterized by PXRD and PND measurements. Pawley fitting the PXRD pattern indicated a space group of $P2_1/c$. Pawley fits were then used to extract the symmetry and unit cell parameters for Co(OH)(sorb) for both the 100 K and 6.71 K patterns [41]. The Pawley fit using the $P2_1/c$ model gave unsatisfactory fit statistics (Fig. S2 $R_{exp}$ = 0.404%, $R_{wp}$ = 1.06%, $R_p$ = 1.76%, and GOF = 2.62). Upon close inspection of the pattern and Pawley fit, three small Bragg peaks remained unfit using the $P2_1/c$ nuclear model which are unresolved in the PXRD pattern. These Bragg peaks were assumed to arise from diffraction from the Co(OH)(sorb) sample and not from possible impurities. The maximal subgroups for the $P2_1/c$ space group were investigated using the online software package ISODISTORT [42,43]. Using this tool, an improved Pawley fit to the experimental data was found using a unit cell with space group $P2_1$ (Fig. S2, top; $R_{exp}$ = 0.400%, $R_{wp}$ = 0.767%, $R_p$ = 1.50, GOF = 1.92). The overall cell parameters remained similar ($V$ = 694.42 (9) Å$^3$ for the $P2_1$ model compared to $V$ = 710.9(3) Å$^3$ for the $P2_1/c$ model), however, the asymmetric unit was doubled in this new, lower symmetry cell. It is possible that the PND measurements conducted at the SNS resolve minor disorder of the O atoms of H atoms unresolved by the in-house powder X-ray diffractometer, leading to the lower symmetry cell obtained in the Pawley fit of the neutron data. The improved fit indicated to us that the $P2_1$ model is a valid description of the unit cell. To decrease the degrees of freedom, the sorbate molecules were introduced as rigid bodies described in a Z-matrix notation [44]. The occupancies of all atoms were fixed at unity. The Rietveld refinements placed significant non-zero intensity at the peaks previously unfit by the $P2_1/c$ Pawley fit of the data. Finally, an improved fit was obtained when

**Table 1**
Unit cell parameters and selected bond lengths and angles. Values in parentheses indicate ±1σ.

| | *a* (Å) | b (Å) | c (Å) | *β* (°) | *V* (Å$^3$) |
|---|---|---|---|---|---|
| 100 K | 6.5584(6) | 6.3255(5) | 16.837(1) | 89.70(1) | 698.5(1) |
| 6.71 K | 6.5566(5) | 6.3124(4) | 16.796(1) | 89.532(8) | 695.13(9) |
| Bond lengths at 6.71 K (Å) | | | | | |
| $Co_a$–OH | 2.0(1), 2.3(1), 2.4(1) | | $Co_a$–sorb | 1.8(1), 2.6(1) | |
| $Co_b$–OH | 1.9(1), 2.3(1), 2.3(1) | | $Co_b$–sorb | 1.7(1), 2.6(1) | |
| ∠(Co–O–Co) angle at 6.71 K (°) | | | | | |
| Diamond plaquette | 101(4), 102 (4) | Octagonal plaquette | 98(1), 100(1), 144(5), 150(5) | | |

the atomic coordinates of the atoms in the ligands were allowed to refine freely instead of being constrained in a rigid body (Fig. 2). Crystallographic information files (CIFs) of the structures at 100 K and 6.71 K are deposited in the CCDC (CCDC deposition numbers 2238233–2238234).

After completing a Rietveld refinement for the PND pattern collected at 100 K, the data collected at 6.71 K were analyzed. Using the CMPR software package, a difference curve was generated by subtracting the 100 K data set from the 6.71 K data set. Inspection of the difference curve revealed that there were no additional Bragg peaks in the PND pattern below $T_N$, unfortunately precluding a structure solution of any anticipated long-range ordered magnetic structure. We observe non-ideal backgrounds at low values of Q, which may arise from structural disorder or possibly from the incoherent scattering from the protiated ligands compounded by the geometry of the POWGEN time-of-flight diffractometer. The structural models obtained from Rietveld refinements of the patterns collected at 100 K and 6.71 K are effectively isostructural, with expected differences in the values of the unit cell axes and bond distances caused by normal thermal expansion.

The crystal structure of Co(OH)(sorb) at 100 K as determined by the PND measurements is shown in Fig. 3, which is related to the brucite-type structure of *β*-$Co(OH)_2$, with one $OH^-$ group replaced by a sorbate ligand (Figs. 1 and 3). This replacement results in an interlayer separation of 16.837(1) Å along the crystallographic *c*-axis, with 2D inorganic layers propagating along the crystallographic *ab*-plane. The layers comprise diamond-shaped and octagonal plaquettes of Co and $\mu_3$-OH moieties formed from highly distorted square pyramidal Co coordination environments. Each metal center is coordinated by three $\mu_3$-$OH^-$ groups within the plane and by two sorbate ligands, one above and one below the all-inorganic plane (Fig. 3). Table 1 summarizes the unit cell values, and selected bond distances and angles in Co(OH)(sorb) observed at 100 K and 6.71 K. At 6.71 K, the Co–OH bond distances are 2.0(1) Å, 2.3(1) Å, and 2.4(1) Å for $Co_a$; and 1.9(1) Å, 2.3(1) Å, and 2.3 (1) Å for $Co_b$. The Co-$O_{sorbate}$ bond lengths are 1.7(1) Å and 1.8(1) Å, with longer contacts of 2.6(1) Å for both $Co_a$ and $Co_b$, arising from the tilted nature of the ligands coordinating the Co–OH layers. The ∠(Co–O–Co) angles in the diamond-shaped plaquette are 101(4) ° and 102(4) °, and in the octagonal plaquette the ∠(Co–O–Co) angles are 98 (1)°, 100(1)°, 144(5)°, and 150(5)°.

Based on the Goodenough-Kanamori-Anderson rules for superexchange, we expect that there may be competing ferro- and antiferromagnetic exchange interactions within the layers based on the∠ (Co–O–Co) angles near 90° and the angles closer to 180°, respectively [45–47]. Competing exchange interactions stemming from the bond angles in the octagonal plaquette may position Co(OH)(sorb) in proximity to a ferrimagnetic state. In comparison, the bond lengths and angles in cubic Brucite-like *β*-$Co(OH)_2$ are 2.117(1) Å and 97.40(7)°, respectively, which promotes ferromagnetic superexchange within the layers. The Co-hydroxyl layers are spaced by 4.6341(1) Å and antiferromagnetic coupling arises between these layers, giving rise to the overall antiferromagnetic structure [48].

To study the effects that the distorted Co geometry may have on the magnetic properties in Co(OH)(sorb), we measured the magnetic susceptibility and magnetization curves at various temperatures. A plot of the magnetic susceptibility data for Co(OH)(sorb) from 5 K to 300 K is shown in Fig. 4. A peak in the zero-field-cooled (ZFC) data corresponds to the Néel temperature at $T_N = 41.7$ K. Bifurcation of the ZFC and field-cooled (FC) data suggests possible field-induced ferrimagnetism. The susceptibility decreases upon increasing the temperature, which reduces the possibility of temperature-independent Van Vleck Paramagnetism. A linear fit to the high temperature region of the inverse susceptibility data

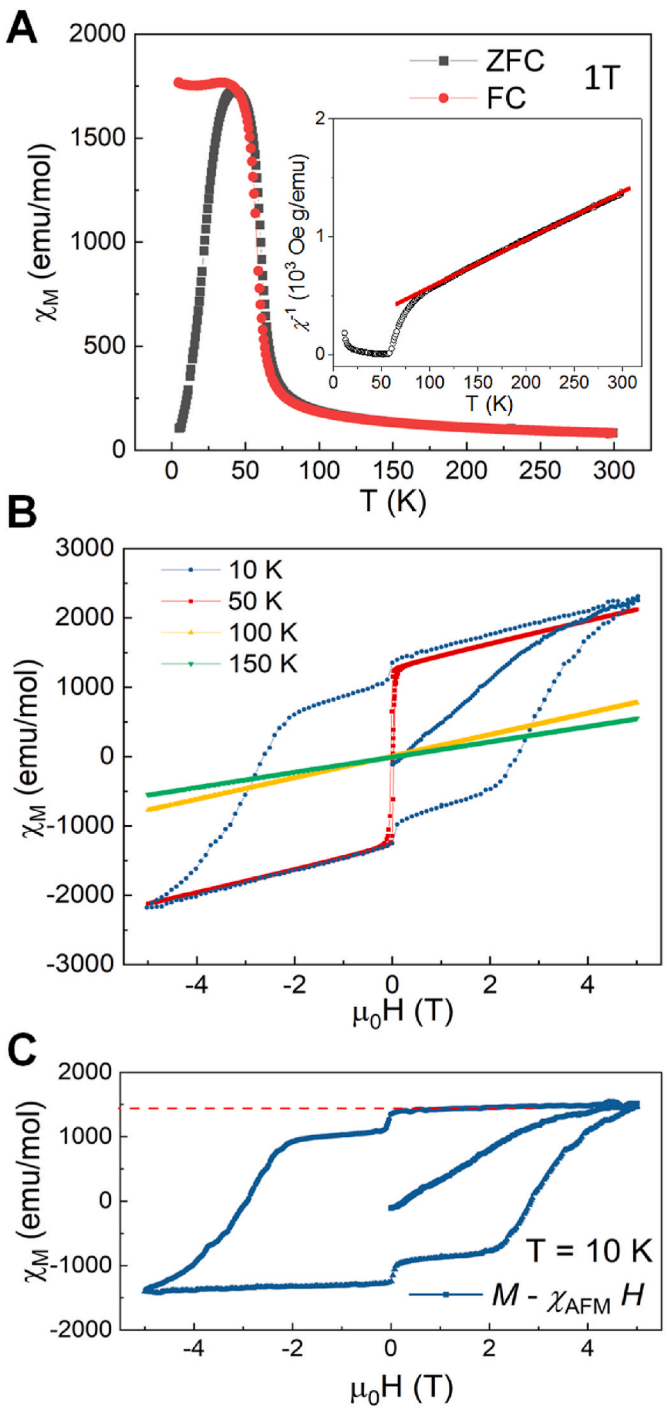


**Fig. 4.** Temperature dependence of the magnetic susceptibility of Co(OH)(sorb) under a field of 1 T. ZFC: Zero-field-cooled (black) and FC: Field-cooled (red) and the inverse magnetization plot (inset). Magnetic hysteresis (B) for Co(OH)(sorb) at various temperatures. Saturation moment after subtracting the linear antiferromagnetic contribution at 10 K (C).

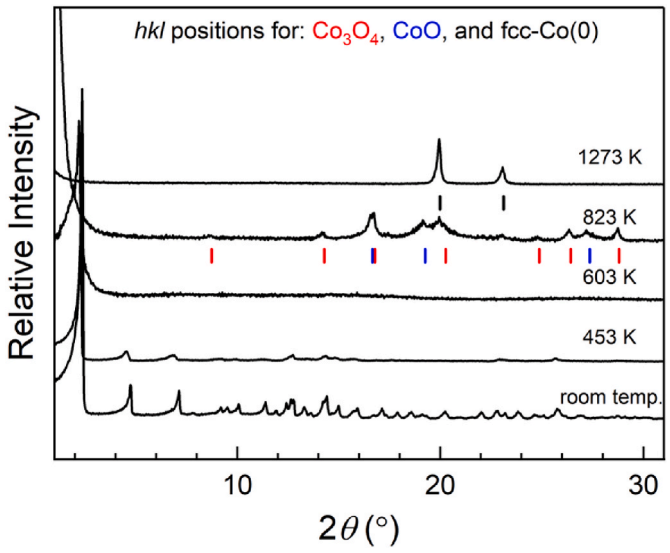


**Fig. 5.** PXRD patterns of thermally decomposed Co(OH)(sorb) samples with *hkl* positions for CoO (red tick marks), $Co_3O_4$ (black tick marks), and fcc Co(0) (blue tick marks).

($T > 100$ K), yields a Curie Weiss temperature of $\theta_{CW} = -20$ K, consistent with a weakly antiferromagnetic state, possibly in proximity to a ferrimagnetic state. From these data, we find an effective magnetic moment of $\mu_{eff} = 3.79\ \mu_B$/Co according to the relationship $C = \mu_0\mu_{eff}^2/\ 3k_B$.

To further investigate the proximity to a field-induced ferrimagnetic state, we measured magnetization curves for Co(OH)(sorb) at various temperatures between −5 T and 5 T. Magnetic hysteresis is observed at 10 K, as shown in Fig. 4. However, the magnetization does not saturate at high magnetic fields but instead shows a linear dependence on the magnetic field $H$, suggesting an antiferromagnetic state. The hysteresis loop is suppressed with increasing temperature and eventually disappears above 50 K, demonstrating paramagnetism above $T_N$. For a high-purity phase, this special kind of *M-H* behavior is consistent with the canted antiferromagnetic states in which the ferromagnetic contribution arises from the field-canted magnetic moments of the Co(II) ions.

To extract the saturation moment, the *M-H* curves were fitted using $M(H) = M_S + M_{AFM}$, where $M_S$ is the saturation moment that is field independent and $M_{AFM}$ is the antiferromagnetic contribution that has a linear relation to the magnetic field,

$$M_{AFM} = \chi_{AFM} \times H$$

The contracted saturation magnetization is shown in Fig. 4c, where the moment of the ferromagnetic components in our canted AFM system is subtracted from the overall saturation magnetization of 0.13 $\mu_B$/Co. This value is smaller than the effective moment calculated from the Curie-Weiss law, which further supports the hypothesized canted antiferromagnetism. It is unlikely that this small a moment could be resolved from the powder neutron diffraction data.

Lastly, the hybrid structure of Co(OH)(sorb) presents an interesting template for thermal synthesis of metallic cobalt nanoparticles [36]. Thermal treatment of Co(OH)(sorb) under a nitrogen atmosphere results in stepwise mass loss, as shown in the TGA curve (Fig. S4). The first step corresponds to mass losses of 6% centered at 423 K, and the second step to an additional 6% loss at 583 K. A larger loss of 48% is observed up to temperatures of 823 K. A final mass loss was observed after this step, which resulted in a residual weight of 33%, approximately the mass of cobalt in the sample.

To better understand the thermal decomposition, we collected PXRD patterns on samples heated to 453 K, 603 K, 823 K, and 1273 K (Fig. 5), corresponding to temperatures after steps in the TGA curve. The PXRD pattern collected after the first mass loss exhibits a pronounced decrease in crystallinity, but indicates overall retention of the crystal packing, particularly along the (001) crystallographic plane perpendicular to the 2D inorganic layers. The second mass loss causes amorphization of the sample, exhibiting only the (001) reflection. We hypothesize that these mass losses correspond to two-step degradation of the organic layer. Further heating to 823 K leads to the formation of a mixture of $Co_3O_4$ and CoO oxides, which corresponds to the 60% total mass losses. Finally, after heating at 1273 K, we observe only the sharp diffraction peaks of *fcc* Co(0). SEM images of the decomposition product at 603 K and 1273 K showed that the crystals appeared progressively more distorted as the sample was heated, while still retaining the general morphology of the 2 μm–5 μm bundled clusters (Fig. 6) [49]. The resulting fcc-phase metallic cobalt, embedded in amorphous carbon, could be useful in catalysis, for reactions such as Fischer-Tropsh [50] or carbon dioxide methanation, and further studies are underway in our laboratory [51].

## 4. Conclusions

The hybrid hydroxide Co(OH)(sorb) was prepared using a hydrothermal method, which resulted in pink, bundled plate microcrystals. The material was structurally characterized with powder diffraction measurements using neutron and X-ray radiation. The crystal structure solution and refinement were performed using PXRD and PND data sets. While both data sets lead to identical crystal packing and connectivity that was described in the $P2_1/c$ space group, only the PND revealed structural details that allowed lowering of the symmetry to $P2_1$. This result emphasizes the need for neutron experiments for detailed structural characterization of hydrocarbon-rich materials, such as emerging class of layered hybrid metal hydroxides. Co(OH)(sorb) was shown to have a distorted brucite-type structure within the inorganic, 2D layer. The layers are pillared by the sorbate ligands, which are bidentate, monotopic, unsaturated linkers, situated in a regular, tightly packed array, with individual layers connected to each other via van der Waals interactions. There are two crystallographically unique Co ions in the asymmetric unit, with highly distorted, square pyramidal local geometries. A preliminary magnetostructural analysis suggests proximity to a ferrimagnetic state. This analysis was corroborated by magnetometry measurements, which indicate that the material is a canted antiferromagnet with $T_N = 41.7$ K Upon heating, the material undergoes a conversion to a mixture of cobalt oxides, then further to metallic cobalt. These results augment the literature of layered hybrid metal hydroxide materials and help shed light on the relationship between dimensionality and magnetism in this class of materials.

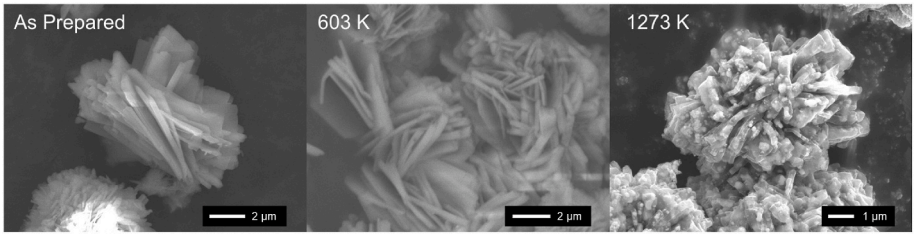


**Fig. 6.** SEM images of Co(OH)(sorb) as synthesized, after heating to 603 K, and after heating to 1273 K.

## Author contributions

The manuscript was written through contributions of all authors. All authors have given approval to the final version of the manuscript.

## Declaration of competing interest

The authors declare that they have no known competing financial interests or personal relationships that could have appeared to influence the work reported in this paper.

## Data availability

Data will be made available on request.

## Acknowledgment

The authors thank Dr. Rita Economos's group from the SMU Roy M. Huffington Department of Earth Sciences for technical assistance. A portion of this research used resources at the Spallation Neutron Source, a DOE Office of Science User Facility operated by the Oak Ridge National Laboratory. The views expressed in the article do not necessarily represent the views of the DOE or the U.S. Government. The U.S. Government retains and the publisher, by accepting the article for publication, acknowledges that the U.S. Government retains a nonexclusive, paid-up, irrevocable, worldwide license to publish or reproduce the published form of this work, or allow others to do so, for U.S. Government purposes. T.R. acknowledges the support from the Robert A. Welch Foundation (Grant No: N-2012-20220331). R.A.K. acknowledges the U. S. DOE Office of Energy Efficiency and Renewable Energy (EERE), Hydrogen and Fuel Cell Technologies Office (HFTO) contract no. DE-AC36-8GO28308 to the National Renewable Energy Laboratory (NREL) and C.M.B. appreciates support from the National Institute of Standards and Technology. W. L. and B. L. acknowledges the supported by US Air Force Office of Scientific Research Grant No. FA9550-19-1-0037, National Science Foundation (NSF)- DMREF- 1921581 and Office of Naval Research Grants No. N00014-22-1-2755 and N00014-23-1-2020.

## Appendix A. Supplementary data

Supplementary data to this article can be found online at https://doi.org/10.1016/j.jpcs.2023.111568.

## References

[1] J. Chen, F. Cheng, Combination of lightweight elements and nanostructured materials for batteries, Acc. Chem. Res. 42 (6) (2009) 713–723.
[2] J.E. ten Elshof, H. Yuan, P. Gonzalez Rodriguez, Two-dimensional metal oxide and metal hydroxide nanosheets: synthesis, controlled assembly and applications in energy conversion and storage, Adv. Energy Mater. 6 (23) (2016), 1600355.
[3] M. Xu, M. Wei, Layered double hydroxide-based catalysts: recent advances in preparation, structure, and applications, Adv. Funct. Mater. 28 (47) (2018), 1802943.
[4] Z.-z. Yang, C. Zhang, G.-m. Zeng, X.-f. Tan, H. Wang, D.-l. Huang, K.-h. Yang, J.-j. Wei, C. Ma, K. Nie, Design and engineering of layered double hydroxide based catalysts for water depollution by advanced oxidation processes: a review, J. Mater. Chem. 8 (8) (2020) 4141–4173.
[5] G. Chen, H. Wan, W. Ma, N. Zhang, Y. Cao, X. Liu, J. Wang, R. Ma, Layered metal hydroxides and their derivatives: controllable synthesis, chemical exfoliation, and electrocatalytic applications, Adv. Energy Mater. 10 (11) (2020), 1902535.
[6] M. Guan, Q. Wang, X. Zhang, J. Bao, X. Gong, Y. Liu, Two-dimensional transition metal oxide and hydroxide-based hierarchical architectures for advanced supercapacitor materials, Front. Chem. 8 (2020) 390.
[7] C. Sanchez, K.J. Shea, S. Kitagawa, Recent progress in hybrid materials science, Chem. Soc. Rev. 40 (2) (2011) 471–472.
[8] P. Rabu, M. Drillon, Layered organic–inorganic materials: a way towards controllable magnetism, Adv. Eng. Mater. 5 (4) (2003) 189–210.
[9] W. Li, J. Wu, S.S. Lee, J.D. Fortner, Surface tunable magnetic nano-sorbents for carbon dioxide sorption and separation, J. Chem. Eng. 313 (2017) 1160–1167.
[10] A. Khayyami, M. Karppinen, Reversible photoswitching function in atomic/molecular-layer-deposited ZnO:azobenzene superlattice thin films, Chem. Mater. 30 (17) (2018) 5904–5911.
[11] T. Deng, W. Zhang, O. Arcelus, J.-G. Kim, J. Carrasco, S.J. Yoo, W. Zheng, J. Wang, H. Tian, H. Zhang, X. Cui, T. Rojo, Atomic-level energy storage mechanism of cobalt hydroxide electrode for pseudocapacitors, Nat. Commun. 8 (1) (2017).
[12] X. Wang, H. Li, J. Lin, C. Wang, X.-L. Wang, Capped keggin type polyoxometalate-based inorganic–organic hybrids involving in situ ligand transformation as supercapacitors and efficient electrochemical sensors for detecting Cr(VI), Inorg. Chem. 60 (24) (2021) 19287–19296.
[13] M. Kurmoo, H. Kumagai, A novel class of layered molecular antiferromagnets, Mol. Cryst. Liq. Cryst. 376 (1) (2002) 555–565.
[14] M. Kurmoo, H. Kumagai, S.M. Hughes, C.J. Kepert, Reversible guest exchange and ferrimagnetism ($T_C$ = 60.5 K) in a porous cobalt(II)-Hydroxide layer structure pillared with trans-1,4-cyclohexanedicarboxylate, Inorg. Chem. 42 (21) (2003) 6709–6722.
[15] W. Roth, Magnetic structures of MnO, FeO, CoO, and NiO, Phys. Rev. 110 (6) (1958) 1333.
[16] M. Yin, X. Wang, W. Mi, G. Chen, B. Yang, A first-principles prediction on the magnetism in CoO with Co and O vacancies, J. Alloys Compd. 610 (2014) 422–427.
[17] J.R. Neilson, J.A. Kurzman, R. Seshadri, D.E.s. Morse, Cobalt coordination and clustering in α-$Co(OH)_2$ revealed by synchrotron X-ray total scattering, Chem. Eur J. 16 (33) (2010) 9998–10006.
[18] X. Liu, W. Liu, W. Hu, S. Guo, X. Lv, W. Cui, X. Zhao, Z. Zhang, Giant reversible magnetocaloric effect in cobalt hydroxide nanoparticles, Appl. Phys. Lett. 93 (20) (2008), 202502.
[19] P. Shamba, R. Zeng, J. Wang, S. Dou, A sign of field-induced first order magnetic state transition and giant reversible magnetocaloric effect in cobalt hydroxide nanosheets, J. Appl. Phys. 107 (9) (2010), 09A919.
[20] M. Okubo, M. Enomoto, N. Kojima, Reversible photomagnetism in a cobalt layered compound coupled with photochromic diarylethene, Solid State Commun. 134 (11) (2005) 777–782.
[21] P.M. Forster, M.M. Tafoya, A.K. Cheetham, Synthesis and characterization of $Co_7(OH)_{12}(C_2H_4S_2O_6)(H_2O)_2$ - a single crystal structural study of a ferrimagnetic layered cobalt hydroxide, J. Phys. Chem. Solid. 65 (1) (2004) 11–16.
[22] M. Kurmoo, Ferrimagnetism in dicarboxylate-bridged cobalt hydroxide layers, J. Mater. Chem. 9 (10) (1999) 2595–2598.
[23] M. Kurmoo, Magnetic ordering in layered cobalt-hydroxide triangular lattices, Mol. Cryst. Liq. 341 (2) (2000) 395–406.
[24] M. Kurmoo, Hard magnets based on layered cobalt hydroxide: the importance of dipolar interaction for long-range magnetic ordering, Chem. Mater. 11 (11) (1999) 3370–3378.
[25] M. Kurmoo, Ferrimagnetic and metamagnetic layered cobalt (II)–Hydroxides: first observation of a coercive field greater than 5 T, Philos. Trans. R. Soc. 357 (1762) (1999) 3041–3061.
[26] X. Liu, R. Ma, Y. Bando, T. Sasaki, High-yield preparation, versatile structural modification, and properties of layered cobalt hydroxide nanocones, Adv. Funct. Mater. 24 (27) (2014) 4292–4302.
[27] V. Oestreicher, D. Hunt, C. Dolle, P. Borovik, M. Jobbágy, G. Abellán, E. Coronado, The missing link in the magnetism of hybrid cobalt layered hydroxides: the odd–even effect of the organic spacer, Chem. Eur J. 27 (3) (2020) 921–927.
[28] Z. Honda, K. Ichimura, K. Saito, T. Kida, M. Hagiwara, Giant hysteretic effect in layered organic-inorganic hybrid magnets incorporating hydroxide and cinnamate layers, Solid State Sci. 123 (2022), 106793.
[29] Z.-L. Huang, M. Drillon, N. Masciocchi, A. Sironi, J.-T. Zhao, P. Rabu, P. Panissod, Ab-initio XRPD crystal structure and giant hysteretic effect ($H_C$ = 5.9 T) of a new hybrid terephthalate-based cobalt(II) magnet, Chem. Mater. 12 (9) (2000) 2805–2812.
[30] A. Debnath, S. Bhattacharya, S.K. Saha, Observation of ferromagnetic ordering in a stable α-$Co(OH)_2$ phase grown on a $MoS_2$ surface, Phys. Rev. B 96 (21) (2017), 214433.
[31] R.K. Feller, B.C. Melot, P.M. Forster, A.K. Cheetham, A hybrid cobalt disulfonate with a novel inorganic layer architecture exhibiting a field-induced magnetic transition, J. Mater. Chem. 19 (17) (2009) 2604.
[32] R. Feyerherm, A. Loose, P. Rabu, M. Drillon, Neutron diffraction studies of canted antiferromagnetic ordering in $Co^{II}$ hydroxide terephtalate, Solid State Sci. 5 (2) (2003) 321–326.
[33] M.L. Główka, D. Martynowski, K. Kozłowska, Stacking of six-membered aromatic rings in crystals, J. Mol. Struct. 474 (1–3) (1999) 81–89.
[34] E. Hadjoudis, Solid-gas reactions. Part V. Bromination of organic solids, in: *Reactivity Of Solids*; Reactivity of Solids, Springer US, 1977, pp. 493–497.
[35] A. Matsumoto, K. Sada, K. Tashiro, M. Miyata, T. Tsubouchi, T. Tanaka, T. Odani, S. Nagahama, T. Tanaka, K. Inoue, others, Reaction principles and crystal structure design for the topochemical polymerization of 1, 3-dienes, Angew. Chem. Int. Ed. 41 (14) (2002) 2502–2505.
[36] A. Eshraghi, A.A. Mirzaei, R. Rahimi, H. Atashi, A simple and low cost method for the synthesis of metallic cobalt nanoparticles without further reduction as an effective catalyst for fischer–tropsch synthesis, React. Kinet. Mech. Catal. 134 (1) (2021) 127–141.
[37] A. Coelho, Topas Academic V6, Coelho Softw., 2017. http://www.topas-academic.net/.
[38] B.H. Toby, CMPR - a powder diffraction toolkit, J. Appl. Crystallogr. 38 (2005) 1040–1041.
[39] A.C. Larson, R.B. Von Dreele, GSAS. Report lAUR (1994) 86–748.
[40] B.H. Toby, J. Appl. Crystallogr. 34 (2001) 210–213.
[41] G.S.J. Pawley, Appl. Crystallogr. 14 (1981) 357–361.
[42] H. T. Stokes, D. M. Hatch, and B. J. Campbell, ISODISTORT, ISOTROPY Software Suite, iso.byu.edu.

[43] H.T. Stokes, D.M. Hatch, B.J. Campbell, D.E. Tanner, ISODISPLACE: a web-based tool for exploring structural distortions, J. Appl. Crystallogr. 39 (4) (2006) 607–614.
[44] R.E. Dinnebier, Rigid bodies in powder diffraction. A practical guide, Powder Diffr. 14 (2) (1999) 84–92.
[45] J.B. Goodenough, Theory of the role of covalence in the perovskite-type manganites [La,M(II)]$MnO_3$, Phys. Rev. 100 (2) (1955) 564–573.
[46] J. Kanamori, Superexchange interaction and symmetry properties of electron orbitals, J. Phys. Chem. Solid. 10 (2–3) (1959) 87–98.
[47] P.W. Anderson, New approach to the theory of superexchange interactions, Phys. Rev. 115 (1) (1959) 2–13.
[48] D. Hunt, G. Garbarino, J.A. Rodríguez-Velamazán, V. Ferrari, M. Jobbagy, D. A. Scherlis, The magnetic structure of -cobalt hydroxide and the effect of spin-orientation, Phys. Chem. Chem. Phys. 18 (44) (2016) 30407–30414.
[49] X. Liu, K.M. Taddei, S. Li, W. Liu, N. Dhale, R. Kadado, D. Berman, C.D. Cruz, B. Lv, Canted antiferromagnetism in the quasi-one-dimensional iron chalcogenide $BaFe_2Se_4$, Phys. Rev. B 102 (18) (2020), 180403.
[50] M.K. Gnanamani, G. Jacobs, W.D. Shafer, B.H. Davis, Fischer–tropsch synthesis: activity of metallic phases of cobalt supported on silica, Catal. Today 215 (2013) 13–17.
[51] T.A. Le, M.S. Kim, S.H. Lee, E.D. Park, CO and CO2 methanation over supported cobalt catalysts, Top. Catal. 60 (9–11) (2017) 714–720.